An improved area-based approach for estimating plot-level tree DBH from airborne LiDAR data

Zhengnan Zhang [a,b], Tiejun Wang [b], Andrew K. Skidmore [b], Fuliang Cao [a], Guanghui She [a], Lin Cao [a,*]

[a] Co-Innovation Center for Sustainable Forestry in Southern China, Nanjing Forestry University, Nanjing, 210037, China
[b] Faculty of Geo-Information Science and Earth Observation (ITC), University of Twente, P.O. Box 217, 7500 AE, Enschede, the Netherlands

ARTICLE INFO

ABSTRACT

The diameter at breast height (DBH) of trees and stands is not only a widely used plant functional trait in ecology and biodiversity but also one of the most fundamental measurements in managing forests. However, systematically measuring the DBH of individual trees over large areas using conventional ground-based approaches is labour-intensive and costly. Here, we present an improved area-based approach to estimate plot-level tree DBH from airborne LiDAR data using the relationship between tree height and DBH, which is widely available for most forest types and many individual tree species. We first determined optimal functional forms for modelling height-DBH relationships using field-measured tree height and DBH. Then we estimated plot-level mean DBH by inverting the height-DBH relationships using the tree height predicted by LiDAR. Finally, we compared the predictive performance of our approach with a classical area-based method of DBH. The results showed that our approach significantly improved the prediction accuracy of tree DBH (R^2 = 0.85–0.90, rRMSE = 9.57%–11.26%) compared to the classical area-based approach (R^2 = 0.80–0.83, rRMSE = 11.98%–14.97%). Our study demonstrates the potential of using height-DBH relationships to improve the estimation of the plot-level DBH from airborne LiDAR data.

1. Introduction

The diameter at breast height (DBH) of trees and stands is not only a widely used plant functional trait in ecology and biodiversity but also one of the most fundamental measurements in forest inventories. DBH has been widely used to estimate forest attributes (e.g. basal area, tree volume, tree volume, biomass, tree size distributions and stand growth) at the individual tree, plot or stand levels (Chang et al., 2015; Şahin et al., 2019; Wu et al., 2019). In addition, DBH has also been used to understand tree vigor and forest structures (Fu et al., 2020), characterize forest dynamics (Wu et al., 2019) and make silvicultural decisions (e.g. rotation age, timber harvest size and assortment) (Saarinen et al., 2017) as well as quantify ecological and economic services of forest ecosystems (Liu et al., 2018). Thus, reliable and up-to-date information on tree DBH is critical to supporting a wide range of sustainable forest management activities (Liang, 2013). Several ground-based tools (e.g. diameter tape, calipers and Biltmore stick) are commonly used to measure the DBH of trees (Mokroš et al., 2018). However, using these techniques to regularly measure the DBH of individual trees over large areas is time-consuming, labour-intensive and expensive (Chave et al., 2005). Consequently, the search for other effective methods for spatially explicit estimates of DBH has long been a key topic in the fields of forest applications (Mokroš et al., 2018; Yang et al., 2020).

Airborne light detection and ranging (LiDAR) technology has recently gained popularity in 3D estimates of forest structures from individual tree level to landscape level (Kankare et al., 2014; Maltamo et al., 2017; Moreira et al., 2021). The most common approach with airborne LiDAR for wall-to-wall estimates of forest structural attributes (e.g. DBH, tree height and basal area) is known as the area-based approach (Ducey, 2012). The area-based approaches are typically based on a statistical model that links LiDAR-derived structural metrics to the field-measured variables in sampled ground plots (White et al., 2013, 2017). As a fundamental unit of the area-based approach, the plot provides more enhanced spatial depictions of forest attributes that can also be summarised to the plot level, allowing for flexibility in updating inventories and avoiding the bias often introduced by the individual tree-based

* Corresponding author.
   E-mail address: lincao@njfu.edu.cn (L. Cao).

approach (Tompalski et al., 2018). Moreover, since the area-based approach is suitable for a lower point cloud density, it is more cost-effective in terms of laser data acquisition and computation. Lefsky et al. (1999) initially laid out the theoretical basis for the area-based approach and provided a practical example. They estimated the plot-level mean DBH (referring to the arithmetic mean value of the diameter of all trees at breast height within a plot, i.e., $(DBH_1 + DBH_2 \ldots + DBH_n)/n)$ of a Douglas fir forest using airborne LiDAR-derived structural metrics and reported an adjusted-R^2 value of 0.61. Hawbaker et al. (2010) used the area-based approach with airborne LiDAR data to predict the plot-level mean DBH of a mixed hardwood forest in eastern North America and achieved an R^2 value of 0.48. In another study, Teobaldelli et al. (2017) estimated the plot-level mean DBH of a Mediterranean forest in southern Italy using the area-based approach and reached an R^2 value of 0.699. Although these studies have demonstrated the feasibility of area-based approaches for estimating the plot-level mean DBH, the estimation accuracy remains relatively low.

Previous studies have shown that there is a strong relationship between tree height and tree DBH, though this relationship is species- (functional-type) and/or site-specific (Temesgen et al., 2014; Jucker et al., 2017; Chenge, 2021). Such a biological relationship between tree height and DBH is significant and has been widely applied in practical forest inventories. For example, the height-DBH relationship has proven to be an effective tool for estimating timber volume and predicting growth and yield (Mensah et al., 2018; Zheng et al., 2018; Cysneiros et al., 2020). Using the height-DBH relationship, researchers also built local height-DBH models to predict the missing tree heights from field-measured DBH to determine volume, biomass and other forest parameters (Ng'andwe et al., 2019). Consequently, numerous height-DBH models have been developed for different tree species using various growth functions in the past (Chenge, 2021). Zhao et al. (2022) demonstrated that the height-DBH model can also be used to estimate individual tree DBH by an inverse of the height-DBH model. However, to the best of our knowledge, no study has applied height-DBH relationships to estimate plot-level DBH from airborne LiDAR data. The height-DBH relationship is not just a statistical expression but has certain biological connotations in some contexts (Bi et al., 2012). We hypothesise that the involvement of this height-DBH biological relationship with airborne LiDAR data could improve the predictive accuracy of plot-level DBH estimates.

In this study, we propose a new area-based approach to estimate plot-level mean tree DBH based on height-DBH relationships using airborne LiDAR data. Specifically, we set out to (1) determine the optimal functional forms for modelling height-DBH relationships for different tree species using field measurements; (2) estimate plot-level mean tree height (referring to the arithmetic mean value of the height of all trees at breast height within a plot, i.e. $(h_1 + h_2 \ldots + h_n)/n)$ and the two parameters of the optimal height-DBH models using airborne LiDAR data; (3) estimate plot-level DBH by inverting the height-DBH relationships using the tree height predicted by LiDAR and compare the predictive performance of the improved area-based approach with a classical area-based approach.

2. Materials and methods

2.1. Study area and tree species

The study was conducted in the Gaofeng Forest Farm (108°23′ E, 22°58′ N) (Fig. 1), a state-operated subtropical planted forest located near the town of Nanning City of Guangxi Province in southwest China. It covers an area of 5200 ha, with elevations ranging from 77 to 463 m above sea level. The main soil type in the study area is lateritic red soil with an average soil layer thickness of over 80 cm. The forest is dominated by Chinese fir (*Cunninghamia lanceolata* (Lamb.) Hook.) and Eucalypt (*Eucalyptus robusta*).

2.2. Data

2.2.1. Field data

The fieldwork was conducted from 16 January to 3 February 2018. We established the plots by considering the indexes of tree species, stand mixture, stand density, tree height, DBH and the topographic effects (i.e. slope and aspect). The existing historical data of stands were used to extract the indexes for stratifying the layers, and then the 49 plots (i.e. Chinese fir ($n = 20$) and eucalypt ($n = 29$)) were finally selected by considering the information in the layers. So these fixed-area square plots across the study site were selected by a stratified sampling strategy in order to cover the range of variability in the attributes for representing the population (White et al., 2013). Each plot was 20 m × 20 m in size, and a Trimble Juno T41/5 Handheld GNSS instrument (Trimble, Sunnyvale, CA, USA) was used to record the centre location of each plot. We measured the height and DBH of all trees with a DBH ≥ 5 cm within each plot using a Vertex IV hypsometer (Haglöf, Långsele, Sweden) and a diameter tape, respectively. Table 1 presents a summary statistic of plot-level mean tree height, DBH and stem density for different species plots.

2.2.2. Airborne LiDAR data

We acquired airborne LiDAR data for the entire study site on 17 and 30 January 2018 using a RIEGL LMS-Q680i long-range airborne laser
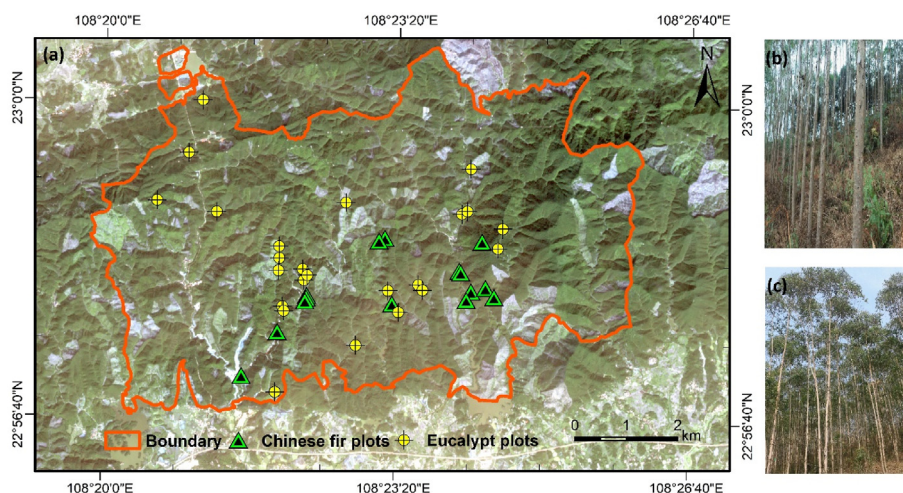

Fig. 1. Map of the study area and the dominant tree species. (**a**) the study area showing the distribution of sample plots; (**b**) Chinese fir forest; and (**c**) eucalypt forest.

Table 1

Summary statistic of field-measured parameters. S.D.: standard deviation.

Plot types	Statistic	Height (m)	DBH (cm)	Stem density (ha^{-1})
Chinese fir plots ($n =$ 20)	Mean	13.3	16.5	1245
	Range	9.7–19.6	11.4–23.3	525–2450
	S.D.	2.4	3.9	523
Eucalypt plots ($n =$ 29)	Mean	15.9	12.6	1641
	Range	8.0–30.4	5.5–23. 5	725–2725
	S.D.	4.6	4.0	576

scanner (RIEGL Laser Measurement Systems, GmbH, Horn, Austria) mounted on a manned fixed-wing aircraft. The aircraft flew 750 m above ground level with a flying speed of 180 km·h^{-1} and a flight line side-lap of 65%. The LiDAR sensor recorded returned waveforms of laser pulses with a temporal sample spacing of 1 ns (approximately 15 cm). The LiDAR system was configured to emit laser pulses in the near-infrared band (1550 nm) at a 300 kHz pulse repetition frequency and an 80 Hz scanning frequency, with a maximum scanning angle of ±30° and a field of view of 60° (RIEGL Laser Measurement Systems, GmbH, Horn, Austria). The average LiDAR point density was 9.58 pulses·m^{-2} and the average beam footprint size was 0.38 m.

After removing outliers of raw point clouds, we first filtered above-ground return points using an improved progressive TIN densification (IPTD) filter algorithm adapted from Zhao et al. (2016). Then, we generated a 1-m digital terrain model (DTM) by calculating the average elevation from the ground points within a rasterised cell grid. If there were no returns within cell grids, these cell grids were filled by inter-polation using an inverse distance weighted (IDW) algorithm. Finally, we normalized the point clouds of the entire study area against the DTM data and extracted point clouds of all sample plots using the coordinates of plot positions. The normalized point clouds of Chinese fir and eucalypt plots are shown in Fig. S1.

2.3. Derivation of LiDAR metrics

We extracted two sets of LiDAR structural metrics, i.e. standard metrics and canopy metrics. The standard metrics consist of height-related metrics (e.g. height percentile, mean height and skewness of heights) and canopy return density-related metrics (e.g. densities, canopy cover and canopy relief ratio). The canopy metrics include several canopy volume (CV) metrics which represent a spatial organisation of the tree material (e.g. trunk and foliage) and the total canopy volume within the canopy, along with others, such as rumple index (Rumple), canopy gap probability (Pgap), coefficient of variation of leaf area density (CvLAD) and vertical complexity index (VCI). The VCI is a scale-independent measure of the evenness of the vertical distribution of the LiDAR point clouds with a scale of 0–1. The closer the VCI value is to 1, the more uniform (i.e. homogeneous) the distribution, and the closer the VCI value is to 0, the more uneven (i.e. heterogeneous) the distribution (van Ewijk et al., 2011). Previous studies have shown that the above-mentioned metrics can provide valuable information in estimating forest structural parameters (Lefsky et al., 1999; Parker et al., 2004; Zhang et al., 2017, 2019; Cao et al., 2019). As a result, a total of 33 LiDAR metrics were generated (Table 2). We calculated these LiDAR metrics in the FUSION (US Forest Service, Seattle, WA, USA) and Matlab R2018b environments (The Mathworks Inc., Natick, Massachusetts, USA).

2.4. Selection of LiDAR metrics

Previous studies have shown that many LiDAR metrics are highly correlated to each other (Silva et al., 2016; Stitt et al., 2022). To avoid potential multicollinearity issues between LiDAR metrics, we first per-formed a variance inflation factor (VIF) analysis and retained the metrics having a VIF value lower than 5 (Peereman and Hogan, 2022). Then, we further calculated the Pearson's correlation coefficients (r) among the

Table 2

Description of the 33 generated LiDAR metrics.

LiDAR metrics	Definition
Standard metrics ($n = 23$)	
h_{25}, h_{50}, h_{75} and h_{95}	The percentiles of the canopy height distributions (25th, 50th, 75th and 95th) of first returns
h_{mean}, h_{max}, h_{SQRT}, h_{CURT}, h_{std}, h_{var}, h_{cv}, $h_{skewness}$ and $h_{kurtosis}$	Mean height, max height, quadratic mean height, cubic mean heights, standard deviation, variance, coefficient of variation skewness and kurtosis of the heights above ground of all first returns
$h_{L\_skewness}$, $h_{L\_kurtosis}$ and h_{L_CV}	The ratio of the third (L3) to the second (L2) L-moments; The ratio of the third (L4) to the second (L2) L-moments; the ratio of the second (L2) to the first (L1) L-moments
d_1, d_3, d_5, d_7 and d_9	The proportion of points above the quantiles (10th, 30th, 50th, 70th and 90th) to total number of points
CC$_{2m}$	Percentages of first returns above 2.0 m
CRR	Canopy relief ratio ((mean − min)/(max − min))
Canopy metrics ($n = 10$)	
Filled, Empty, OG, CG, Eu, Oligo	The voxels filled in point clouds and empty voxels within canopy spaces (Filled, Empty); the empty voxels located above and below the canopy respectively (OG, CG); the voxels located within an uppermost percentile (65%) of filled grid cells of that column and voxels located below the point in the profile (Eu, Oligo)
Rumple	The ratio of canopy outer surface area to ground surface area
P_{gap}	A gap probability measurement using the equation (N_{ground}/N_{total}); N_{ground} is the number of pulses having the last return down to the ground; N_{total} is the total number of all returns
CvLAD	Variation within the vertical leaf area density profile
VCI	Distribution of abundance of returns in specified height bins. VCI $= -\sum_{i=1}^{HB}[p_i \ln(p_i)]/\ln(HB)$, where HB is the total number of height bins, and p_i is the proportional abundance of LiDAR returns in height bin i

remaining metrics using a "corrplot" package in R version 3.6.1 (R Core Team, 2008). We retained the metrics with low correlation ($|r| < 0.7$) (Dormann et al., 2013). Pearson's correlation coefficient confirmed that the $|r|$ values of all pairs of remaining metrics determined by VIF were lower than 0.7 (Fig. 2). As a result, we selected 11 out of 33 LiDAR metrics for use in subsequent prediction models (Table 3).

2.5. Models for DBH estimation

2.5.1. Classical area-based approach

We used a classical area-based approach for plot-level DBH estimates as a comparison of the improved area-based approach proposed in this study. In the classical area-based approach, we established the plot-level statistical regression relationships between LiDAR metrics and field-measured mean DBH using the following formula:

$$D_i = f(X_{im}), i = 1, \cdots, n, n > m, \tag{1}$$

where D_i denotes field-measured mean DBH of plot i, X_{im} denotes the mth LiDAR metrics derived from plot i, f denotes predictive function, either as parametric or non-parametric models.

The random forest (RF) algorithm is one of the most commonly used non-parametric regression approaches for predicting forest attributes in LiDAR-based forest inventory (Belgiu and Drăgu, 2016). One of the main benefits of using the RF algorithm is that multiple predictive variables can be incorporated without making assumptions about their statistical distribution or covariance structure (Belgiu and Drăgu, 2016). Thus, we also employed the RF for estimating DBH in the classical area-based approach. For the RF algorithm, there are two key parameters, i.e. the
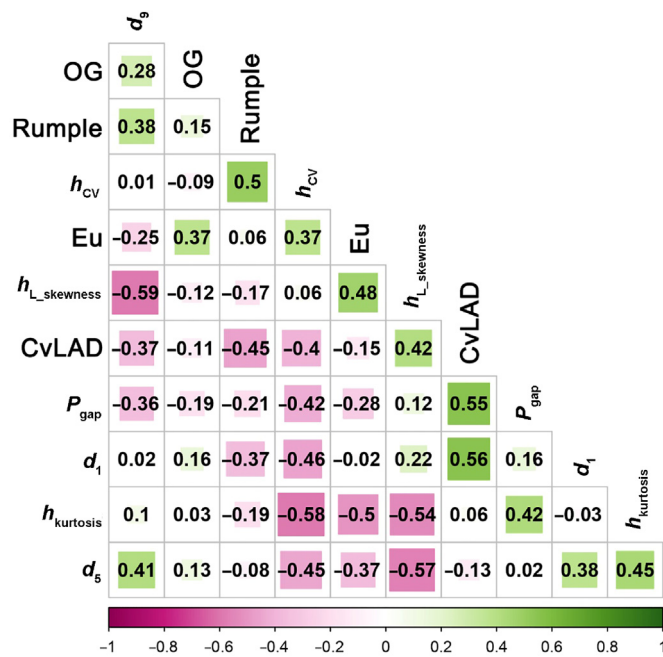
Fig. 2. Cross-correlation matrix of the 11 LiDAR metrics determined by the variance inflation factor (VIF); see Table 3 for definitions of the metrics.

Table 3

Selected LiDAR metrics for DBH estimations in this study based on the variance inflation factor (VIF) analysis.

LiDAR metrics	Definition
h_{cv}	Coefficient of variation of the heights above ground of all first returns
$h_{kurtosis}$	Kurtosis of the heights above ground of all first returns
$h_{L\_skewness}$	Ratio of the third (L3) to the second (L2) L-moments
d_1	Proportion of points above the 10th quantiles to the total number of points
d_5	Proportion of points above the 50th quantiles to the total number of points
d_9	Proportion of points above the 90th quantiles to the total number of points
OG	Empty volume that voxels located above the canopy
Eu	Euphotic volume that voxels located within an uppermost percentile (65%) of filled grid cells of that column
Rumple	The ratio of canopy outer surface area to ground surface area
P_{gap}	A gap probability measurement using the equation (N_{ground}/N_{total}); N_{ground} is the number of pulses having the last return down to the ground; N_{total} is the total number of all returns
CvLAD	Variation within the vertical leaf area density profile

number of decision trees (*ntree*) and the number of variables to randomly sample as candidates at each split (*mtry*), which need to be defined by users. In this study, default settings (*ntree* = 500 and *mtry* = 1/3 of the number of feature variables) were selected to train the RF regression models, since previous studies have shown that the default parameter setting often leads to a more accurate model prediction (Belgiu and Drăgu, 2016; Zhao et al., 2019). We implemented RF model using the *R* package "*randomForest*" in this study. The RF models were constructed using Chinese fir plots, eucalypt plots and pooled plots.

2.5.2. Improved area-based approach

The improved area-based approach consists of several steps (Fig. 3). First, we determined the forms of the optimal fitting functions for modelling field-measured tree height-DBH relationships. To do so, we selected 10 equations (Table 4) with tree height (*H*) and DBH (*D*) as candidate functions (*f*) since previous studies demonstrated these functions have a relatively low unexplained variance when fitting height-DBH

relationships (Huang and Titus, 1992; Tuan et al., 2019). We classified the entire datasets into three different groups (i.e. Chinese fir plots, eucalypt plots and pooled plots) (Table 5). The pooled plots contained the measured individual trees from all plots to establish more reliable height-DBH models and we used their tree heights and DBH values to model height-DBH relationships. We randomly divided the total samples of each group into training (70%) and validation (30%) data sets for developing general height-DBH models and evaluating their performance. We evaluated candidate functions with training data sets to select the best function forms for pooled plots, Chinese fir plots and eucalypt plots, respectively. We used the R^2 (coefficient of determination), RMSE (root-mean-square-error) and rRMSE (relative RMSE) as measures to assess the accuracies of height-DBH models from training data sets and used the MAE (mean absolute error) and MAPE (mean absolute percent error) to evaluate the validation performance of height-DBH models.

After we selected the optimally fitting function forms of general height-DBH models, we used them to fit the height-DBH relationships of each plot. Then, we calculated plot-level β_0 and β_1 by a non-linear least square (NLE) function when modelling the height-DBH relationship of each plot. Next, we estimated plot-level H, β_0 and β_1 by selected LiDAR metrics in RF models. Finally, we estimated the plot-level DBH from an inverse function of LiDAR-reconstructed height-DBH relationships with input variables (i.e. estimated plot-level H, β_0 and β_1) through the following formula:

$$H = f(D), D \in (0, +\infty) \rightarrow D = f^{-1}(H), D \in (0, +\infty), \quad (2)$$

where H and D are LiDAR-predicted tree height and DBH, respectively. f^{-1} is the inverse function of *f*.

2.6. Model accuracy assessment

The performance of the developed plot-level RF models of DBH, H, β_0 and β_1 was evaluated through a leave-one-out cross-validation (LOOCV) analysis, which uses a single observation from the original set as validation data and the remainder as training data. This process was iterated until all observations in the sample set are used once as validation data. Specifically, we repeated the LOOCV process for Chinese fir plots, eucalypt plots and pooled plots 20, 29 and 49 times, respectively. We assessed the predictive performance of each RF model using R^2 and rRMSE (%) within the LOOCV and selected the model with the best performance.

3. Results

3.1. Optimal height-DBH models

Table 6 shows the most accurate general height-DBH models for Chinese fir plots (R^2 = 0.76, RMSE = 1.71, rRMSE = 12.91%), eucalypt plots (R^2 = 0.73, RMSE = 2.51, rRMSE = 16.44%) and pooled plots (R^2 = 0.51, RMSE = 3.34, rRMSE = 22.76%). The height-DBH model for pooled plots produced the lowest accuracy in terms of fitting performance and validation performance (MAE = 2.60, MAPE = 18.87%). The height-DBH model for Chinese fir plots achieved slightly better validation performance (MAE = 1.33, MAPE = 11.06%) than the height-DBH model for eucalypt plots (MAE = 1.94, MAPE = 14.71%).

Fig. 4 shows the optimal height-DBH relationships with the fitted curves for different plot types using logarithmic, linear and Meyer fitting functional forms, respectively.

3.2. Estimation of plot-level mean tree height and the two parameters of the height-DBH models

Table 7 shows the prediction accuracy of plot-level mean tree height and the two parameters of the height-DBH models using airborne LiDAR data. The accuracy of tree height prediction for the pooled plots was the
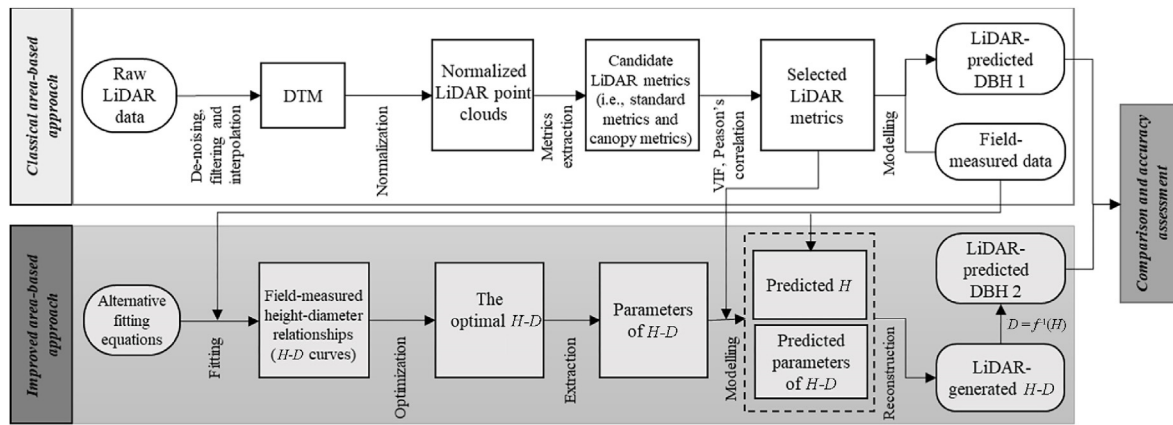
Fig. 3. Outline of the workflow of the study; DTM: digital terrain model, DBH: mean diameter at breast height, *H*: mean tree height, height-DBH: height-DBH relationship. $D = f^{-1}(H)$: DBH's inverse function.

Table 4

Ten candidate height-DBH models evaluated in this study. *H*: tree height (m), *D*: tree diameter at breast height (cm), β_0 and β_1: parameters to be estimated.

Eq. no.	Models	Equations	References
Two-parameters functions: $H = f(D)$			
1	Linear	$H = 1.3 + \beta_0 D + \beta_1$	Mensah et al. (2018)
2	Power	$H = 1.3 + \beta_0 D^{\beta_1}$	Tuan et al. (2019)
3	Exponential	$H = 1.3 + \beta_0 \exp(\beta_1 D)$	Gao et al. (2016)
4	Logarithm	$H = 1.3 + \beta_0 \ln D + \beta_1$	Baral (2017)
5	Wykoff	$H = 1.3 + \exp\left(\beta_0 + \dfrac{\beta_1}{1+D}\right)$	Wykoff et al. (1982)
6	Meyer	$H = 1.3 + \beta_0[1 - \exp(-\beta_1 D)]$	Meyer (1940)
7	Näslund	$H = 1.3 + \left(\dfrac{D}{\beta_0 + \beta_1 D}\right)^2$	Pukkala et al. (1990)
8	Curtis	$H = 1.3 + \beta_0\left(\dfrac{D}{1+D}\right)^{\beta_1}$	Curtis (1967)
9	Bertalanffy	$H = 1.3 + \beta_0[1 - \exp(-\beta_1 D)]^3$	Von Bertalanffy (1949)
10	Hossfeld	$H = 1.3 + \dfrac{\beta_0 D^2}{(\beta_1 + D)^2}$	Sharma (2009)

Table 5

Statistics of the number of training and validation samples in different groups employed for modelling height-DBH relationships.

Groups	Number of total samples	Number of training samples	Number of validation samples
Chinese fir plots ($n = 20$)	851	596	255
Eucalypt plots ($n = 29$)	1817	1272	545
Pooled plots ($n = 49$)	2668	1868	800

highest ($R^2 = 0.89$, rRMSE $= 9.49\%$), followed by eucalypt plots ($R^2 = 0.88$, rRMSE $= 10.36\%$) and Chinese fir plots ($R^2 = 0.83$, rRMSE $= 15.21\%$). For the prediction of the two parameters of the height-DBH models, β_1 generally yielded relatively higher accuracy than β_0. The accuracy of β_0 and β_1 prediction for the pooled plots was the highest ($R^2 =$

0.89–0.96, rRMSE $= 7.16\%$–13.36%), followed by Chinese fir plots ($R^2 = 0.86$–0.89, rRMSE $= 13.08\%$–14.22%) and eucalypt plots ($R^2 = 0.74$–0.78, rRMSE $= 18.78\%$–19.89%).

3.3. Performance comparsion between the classical area-based approach and the improved area-based approach

Fig. 5 shows the field-measured versus LiDAR-estimated mean DBH using the classical area-based and the improved area-based approach for Chinese fir plots, eucalypt plots and pooled plots, respectively. For the classical area-based approach, the prediction accuracy for the eucalypt plots ($R^2 = 0.83$, rRMSE $= 11.98\%$) was slightly higher than that of the Chinese fir plots ($R^2 = 0.80$, rRMSE $= 14.97\%$) and pooled plots. For the improved area-based approach, the prediction accuracy of the DBH for eucalypt plots was the highest ($R^2 = 0.90$, rRMSE $= 9.57\%$), followed by pooled plots ($R^2 = 0.88$, rRMSE $= 10.49\%$) and Chinese fir plots ($R^2 = 0.85$, rRMSE $= 11.26\%$).

In comparison, the improved area-based approach yielded relatively higher accuracy ($R^2 = 0.85$–0.90, rRMSE $= 9.57\%$–11.26%) than the classical area-based approach ($R^2 = 0.80$–0.83, rRMSE $= 11.98\%$–14.97%). Specifically, the prediction accuracy of the DBH for eucalypt plots was significantly higher than that of Chinese fir plots.

4. Discussion

The results of this study showed that the new area-based approach with airborne LiDAR data considerably improved the accuracy ($R^2 = 0.85$–0.90, rRMSE $= 9.57\%$–11.26%) of the DBH estimation at the plot level. This demonstrated the effectiveness of combining the height-DBH relationship with airborne LiDAR data for estimating plot-level DBH.

With classical area-based approaches, most previous studies on estimating plot- or stand-wise DBH have often shown limited performance (e.g. Muhamad-Afizzul et al., 2019; Ozkan et al., 2022). This may be explained by the volatile relationship between the mean DBH and the LiDAR-derived metrics used in the developed models. Due to the "top-to-bottom" scanning mode of airborne LiDAR systems, the LiDAR metrics used to describe stand structure are generally derived from the vertical distribution of LiDAR returns. These metrics often reflect the complexity of the canopy vertical structure whereas most of them do not sufficiently
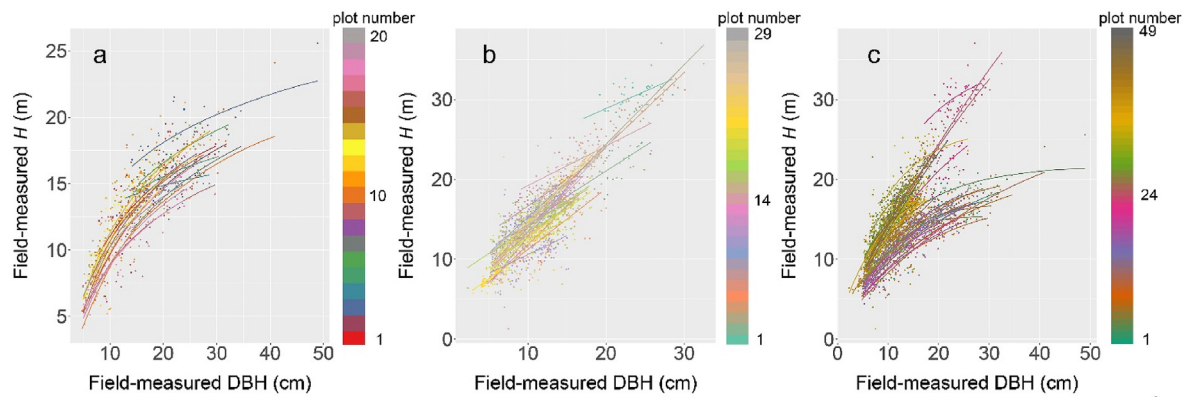
Table 6

The optimal height-DBH models established using field measurements; significance level of *F*-test *p*-value: *$p < 0.05$.

Types	Models	Equations	R^2	RMSE	rRMSE (%)	MAE	MAPE (%)
Chinese fir plots	Logarithm	$H = 1.3 + 6.890\ln D - 6.403$	0.76*	1.71	12.91	1.33	11.06
Eucalypt plots	Linear	$H = 1.3 + 0.960D + 2.497$	0.73*	2.51	16.44	1.94	14.71
Pooled plots	Meyer	$H = 1.3 + 23.967[1 - \exp(-0.067D)]$	0.51*	3.34	22.76	2.60	18.87

Fig. 4. The optimal height-DBH relationships with fitted curves using field measurements; each curve with various colours represents the height-DBH relationship of each plot and this curve was fitted by the selected fitting functional form from Table 6, but plot-level β_0 and β_1 of each curve were recalculated when modelling the height-DBH relationship of each plot; **a**: height-DBH curves of Chinese fir plots fitted by a logarithmic model; **b**: height-DBH curves of eucalypt plots fitted by a linear regression model; **c**: height-DBH curves of pooled plots fitted by a Meyer model. (For interpretation of the references to colour in this figure legend, the reader is referred to the Web version of this article.)

Table 7
Accuracy results of predictive plot-level tree height (H) and two parameters (β_0 and β_1) of the selected height-DBH models for Chinese fir plots, eucalypt plots and pooled plots using LiDAR metrics; significance level of F-test with p-value: *p < 0.05.

LiDAR predictions	Evaluation indexes	Forest types		
		Chinese fir plots	Eucalypt plots	Pooled plots
H	R^2	0.83*	0.88*	0.89*
	rRMSE (%)	15.21	10.36	9.49
β_0	R^2	0.86*	0.74*	0.89*
	rRMSE (%)	13.08	19.89	13.36
β_1	R^2	0.89*	0.78*	0.96*
	rRMSE (%)	14.22	18.78	7.16

take into account horizontal structure arrangement, indicating they are generally more height-related but less diameter-related (Coomes et al., 2017; Moran et al., 2018). Bouvier et al. (2015) and Véga et al. (2016) thus suggested that an area-based approach should consider involving the metrics that have the potential to provide information on plot horizontal heterogeneity. The canopy volume metrics (e.g. OG and Eu) and the Rumple (Fig. 2) employed in our study have been demonstrated to take into account horizontal structure within the model prediction. This may explain why our DBH models generated by the classical approach maintained a relatively high predictive performance (R^2 > 0.80). Another reason explaining these results may be the fact that Chinese fir and eucalypt plots of our research site were established in almost single-layered pure stands with relatively even-sized diameter distributions and such stand structure characteristics, thereby producing a relatively strong relationship between mean DBH and LiDAR data at the plot or stand level (Næsset et al., 2004). In this regard, the classical area-based approach for DBH estimates is more dependent on the characteristics of the input datasets and forest conditions (Moran et al., 2018).

Unlike plot-level mean DBH, mean tree height can be predicted more accurately either in single- or multi-layered forests due to the attribute characteristics of airborne LiDAR itself. In the improved area-based approach, retrieval of mean tree height from airborne LiDAR permits its use in the prediction of mean DBH via the height-DBH models. Substantially, the relationship between tree height and DBH is an inherent functional trait of the tree itself that reflects the evolutionary competition and a balance between tree growth and survival within a stand and this kind of relationship always are biologically interpretable rather than merely understood as a statistical relationship (Chave et al., 2005; Bi et al., 2012). The significant increases in the DBH predictions of our

results may be explained by the fact that our improved area-based approach made DBH predictions no longer directly dependent on the unstable relationship with the LiDAR metrics. Moreover, compared to the classical area-based modeling, our approach gained more mechanistic understanding and interpretability for the DBH predictive models by incorporating intrinsic physiological height-DBH relationships.

We confirmed that the best optimal height-DBH models varied significantly among tree species (Table 6). This is in line with the findings of Cysneiros et al. (2020) and Mensah et al. (2018), who indicated species dependency in height-DBH models. This might be explained by the reason that tree architectural and physiological differences showed to be species-specific. In this case, eucalypt is a fast-growing and high-yielding plantation species and it is highly intensively managed with a shorter rotation than Chinese fir in our study site. Thus, the stable height-DBH relationship with a seemingly constant growth rate in young Eucalypt forests could be well captured linearly, while comparatively, the concave-shaped logarithmic function was selected as the optimal function for Chinese fir plots. Our finding that the species-specific height-DBH models outperformed the generic model (i.e. pooled plots) is not surprising, as these models without consideration of species information might embody much hierarchical and heterogeneous forest structure information and result in large systematic errors (Kearsley et al., 2017; Mensah et al., 2018). As pointed out in Mensah et al. (2018), the generic models can provide a cost-effective (fewer field measurements and inventory efforts) and relatively accurate (for large-scale application) approach but these models are less accurate at local or fine-scale application, especially for species in environments (Kearsley et al., 2017). Thus, to increase the geographical generality and the prediction accuracy of height-DBH models, incorporation of a site (e.g. stand age) and climate variables (e.g. precipitation) could be considered in our future works since these variables have proven to the interactive effects on height-DBH models (Zhang et al., 2018; Sharma et al., 2019; Cui et al., 2022).

The height–diameter relationship of trees in a forest stand can vary by plots with different variations; hence, there is a need to incorporate plot-level height–DBH variations into the models (Chenge, 2021). In this study, we calibrated the height–DBH models of each plot by modulating their β_0 and β_1 values. To do this, our improved area-based approach allowed us to derive localised β_0 and β_1 values of each plot by fitting field-measured data using the optimal height-DBH models and estimate these two parameters by LiDAR metrics. Surprisingly, both β_0 and β_1 yielded high predictive accuracies in our study (Table 7). One potential explanation that could be offered is their strong correlation with tree height. Previous studies have noted that strata-specific predictive models had a positive impact on final estimations compared to unstratified models (Bouvier et al., 2015; Latifi et al., 2015; Zhang et al., 2017, 2019;
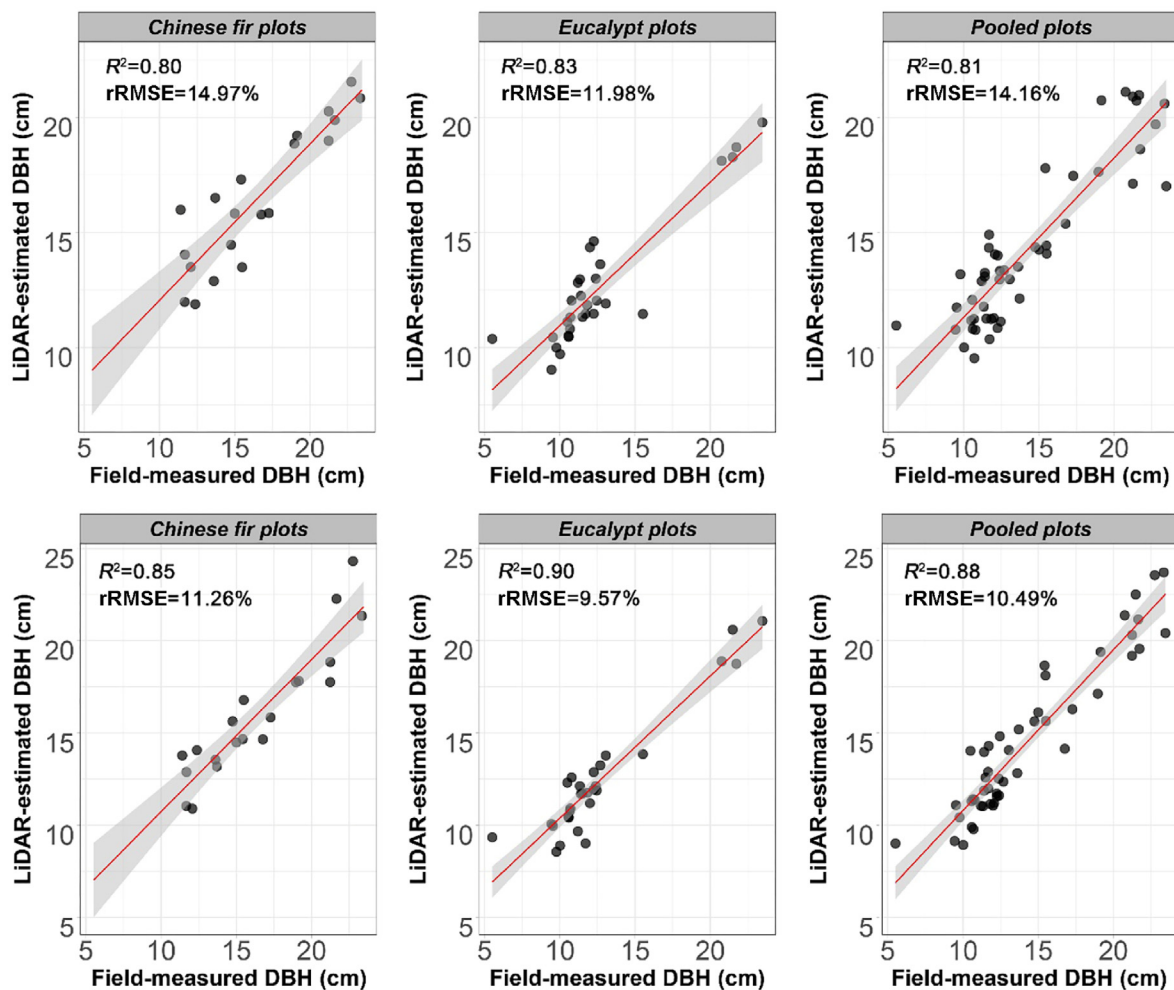
Fig. 5. Field-measured versus LiDAR-estimated plot-level mean DBH using a classical area-based approach (top row) and an improved area-based approach (bottom row), respectively; the grey area represents a 95% confidence interval; all predictive models with a significance level of *F*-test with *p*-value <0.05.

Cao et al., 2019). But such a conclusion is not an absolute one. Latifi et al. (2015) reported only slight improvements when using forest-type stratification for biomass estimations. The outcomes that unstratified models showed higher performance than stratified models were also reported by Hollaus et al. (2007), Tonolli et al. (2011) and Mcroberts et al. (2013), which were similar with our results (Table 7). Our predictive β_0 and β_1 models of the pooled plots in Table 7 had relatively higher performance than those of the species-specific plots. However, it might also be noted that both β_0 and β_1 of species-specific plots and pooled plots were conferred different biological meanings depending on the their selected allometric *H-D* models. For instance, the β_0 of Meyer is an asymptote parameter representing the maximum attainable tree height, whereas the β_0 (i.e. slope term) of Linear function for eucalypt plots represents the increment rate of tree height with diameter and the Logarithm function's β_0 of Chinese fir plots is actually a scale parameter, which could control the scale size (i.e. height range) of the curve distributions. The β_0 of Meyer for pooled plots could be more directly related to the tree height and therefore it was well predicted by the LiDAR metrics than the β_0 of species-specific plots. For *H* estimations, the *H* model of Chinese fir plots obtained the lowest prediction accuracy in our results. This may be due to the fact that Chinese fir forests had more uneven-sized stands and possessed higher inequality of tree size than Eucalypt forests and their sharp treetops were difficult to be hit by narrow laser pulses due to their unique conical crowns, resulting in an underestimate of *H* and an unapparent accuracy improvement of stratified Chinese fir models compared to the general models of pooled plots. The *H* model of pooled

plots performed better that of eucalypt plots. One reason for explaining this may be the fact that there was variability between the plot species, but lower intra plot variability in pooled plots (e.g. standard deviation of field-measured *H* = 4.2 m) compared to eucalypt plots (e.g. standard deviation of field-measured *H* = 4.6 m).

To our knowledge, no study has estimated two parameters of height-DBH models at the plot level using LiDAR metrics. This study provides new insights as our area-based approach calibrated height-DBH models of each plot and consequently improved plot-level DBH estimates by an inversion of these localised height-DBH models and LiDAR-predicted mean tree heights. This manner can help specific areas to achieve plot-specific height-DBH models and magnitude and spatial distribution mapping of wall-to-wall DBH using the improved area-based approach, which will contribute to the understanding of stand growth and support precise silviculture and sustainable management across varied forest stands in subtropical planted forests. However, an accurate mapping of tree species classification is also an essential prerequisite for spreading the improving area-based approach to extrapolate plot-wise DBH over larger coverage. Therefore, future studies should endeavor to make some potential improvements, such as coupling those optical spectral indices that greatly favor tree species classification into our approach. In addition, since our study was conducted in a plantation area with relatively homogeneous canopy vertical structures, the promotion and large-scale application of our approach still requires further verification in forests with more complex structures, such as natural forests. Moreover, in our study, the localized *H-D* relationships were determined by in-situ

measurements of individual tree DBH and tree height, which is labour intensive and also costly. In recent years, UAV-borne LiDAR has become particularly notable in enhanced forest inventories due to its light weight, low cost, flight route flexibility and high repeatability etc. (Gao and Zhang, 2021). UAV-borne LiDAR systems can accurately measure tree height by high density point clouds (Puliti et al., 2020; Corte et al., 2020). Terrestrial LiDAR and Mobile LiDAR (e.g. backpack or hand-held) systems have excellent advantages in estimating tree DBH because they have the strong capability to characterize 3D under-canopy structures (e.g. tree trunks and branches) (Liang et al., 2019). Thus, if we want to establish the localized height-DBH models without using in-situ tree height and measurements in the future, we could use the combination of UAV-borne LiDAR data and Terrestrial/Mobile LiDAR data to obtain the fused point clouds (characterizing the complete forest vertical structure), and then extract a sufficient number of individual tree parameters (height (from UAV LiDAR) and DBH (from Terrestrial/Mobile LiDAR)) to establish localized height-DBH models. Once the localized height-DBH models are established, we could finally extrapolate the developed area-based approach in this study for larger coverage using airborne/UAV-borne LiDAR data to make "wall-to-wall" predictions of localized height-DBH models, for predicting DBH in the study site.

5. Conclusions

In this study, we proposed an improved area-based approach for plot-level DBH estimates using airborne LiDAR data based on height-DBH relationships. We also compared the performance of our approach with a classic area-based approach. Results showed that our approach significantly improved the plot-level DBH estimates. In the improved area-based approach, plot-level mean tree height and two parameters (i.e. β_0 and β_1) of height-DBH models were predicted with good accuracies, which greatly contributed to the improvements of plot-level DBH estimates. Our approach can help foresters acquire DBH products at the plot level that meet the demands of the forestry industry in a LiDAR-aided forest inventory, which could improve our understanding of the ecological functions of forests, improve forest treatments and support sustainable forest management.

Authors' contributions

Conceptualization, Z.Z., T.W. and L.C.; methodology, Z.Z.; formal analysis, Z.Z.; investigation, Z.Z., L.C. and G.S.; writing—original draft preparation, Z.Z. and T.W.; writing—review and editing, T.W., A.K.S. and L.C.; visualization, Z.Z. and T.W.; supervision, T.W., A.K.S. and F.C. All authors have approved the manuscript and agreed with its submission to *Forest Ecosystems*.

Data availability

Not applicable.

Declaration of competing interests

The authors declare that they have no known competing financial interests or personal relationships that could have appeared to influence the work reported in this paper.

Appendix A. Supplementary data

Supplementary data to this article can be found online at https://doi.org/10.1016/j.fecs.2023.100089.

References

Baral, S., 2017. Modeling height-diameter relationship and volume of teak (*Tectona grandis* L. F.) in central lowlands of Nepal. J. Trop. For. Environ. 07, 28–42. https://doi.org/10.31357/jtfe.v7i1.3020.

Belgiu, M., Drăgu, L., 2016. Random forest in remote sensing: a review of applications and future directions. ISPRS J. Photogrammetry Remote Sens. 114, 24–31. https://doi.org/10.1016/j.isprsjprs.2016.01.011.

Bi, H., Fox, J.C., Li, Y., Lei, Y.C., Pang, Y., 2012. Evaluation of nonlinear equations for predicting diameter from tree height. Can. J. For. Res. 42, 789–806. https://doi.org/10.1139/X2012-019.

Bouvier, M., Durrieu, S., Fournier, R.A., Renaud, J.P., 2015. Generalizing predictive models of forest inventory attributes using an area-based approach with airborne LiDAR data. Remote Sens. Environ. 156, 322–334. https://doi.org/10.1016/j.rse.2014.10.004.

Cao, L., Zhang, Z., Yun, T., Wang, G., Ruan, H., She, G., 2019. Estimating tree volume distributions in subtropical forests using airborne LiDAR data. Rem. Sens. 11, 97. https://doi.org/10.3390/rs11010097.

Chang, A., Jung, J., Kim, Y., 2015. Estimation of forest stand diameter class using airborne lidar and field data. Remote Sens. Lett. 6, 419–428. https://doi.org/10.1080/2150704X.2015.1035770.

Chave, J., Andalo, C., Brown, S., Cairns, M.A., Chambers, J.Q., Eamus, D., Fölster, H., Fromard, F., Higuchi, N., Kira, T., Lescure, J.-P., Nelson, B.W., Ogawa, H., Puig, H., Riéra, B., Yamakura, T., 2005. Tree allometry and improved estimation of carbon stocks and balance in tropical forests. Oecologia 145, 87–99. https://doi.org/10.1007/s00442-005-0100-x.

Chenge, I.B., 2021. Height–diameter relationship of trees in Omo strict nature forest reserve, Nigeria. Trees For. People 3, 100051. https://doi.org/10.1016/j.tfp.2020.100051.

Corte, A.P.D., Rex, F.E., de Almeida, D.R.A., Sanquetta, C.R., Silva, C.A., Moura, M.M., Wilkinson, B., Zambrano, A.M.A., da Cunha Neto, E.M., Veras, H.F.P., de Moraes, A., Klauberg, C., Mohan, M., Cardil, A., Broadbent, E.N., 2020. Measuring individual tree diameter and height using gatoreye high-density UAV-Lidar in an integrated crop-livestock-forest system. Remote Sens. 12 (5), 863. https://doi.org/10.3390/rs12050863.

Coomes, D.A., Dalponte, M., Jucker, T., Asner, G.P., Banin, L.F., Burslem, D.F.R.P., Lewis, S.L., Nilus, R., Phillips, O.L., Phua, M.H., Qie, L., 2017. Area-based vs tree-centric approaches to mapping forest carbon in Southeast Asian forests from airborne laser scanning data. Remote Sens. Environ. 194, 77–88. https://doi.org/10.1016/j.rse.2017.03.017.

Cui, K., Wu, X., Zhang, C., Zhao, X.H., von Gadow, K., 2022. Estimating height-diameter relations for structure groups in the natural forests of Northeastern China. For. Ecol. Manag. 519, 120298. https://doi.org/10.1016/j.foreco.2022.120298.

Curtis, R.O., 1967. Height-diameter and height-diameter-age equations for second-growth douglas-fir. For. Sci. 13, 365–375. https://doi.org/10.1093/forestscience/13.4.365.

Cysneiros, V.C., Pelissari, A.L., Gaui, T.D., Fiorentin, L.D., de Carvalho, D.C., Borges, T., Filho, S., Machado, S.d.A., 2020. Modeling of tree height–diameter relationships in the atlantic forest: effect of forest type on tree allometry. Can. J. For. Res. 50, 1289–1298. https://doi.org/10.1139/cjfr-2020-0060.

Dormann, C.F., Elith, J., Bacher, S., Buchmann, C., Carl, G., Carre, G., Marquez, J.R.G., Gruber, B., Lafourcade, B., Leitao, P.J., Munkemuller, T., McClean, C., Osborne, P.E., Reineking, B., Schroder, B., Skidmore, A.K., Zurell, D., Lautenbach, S., 2013. Collinearity: a review of methods to deal with it and a simulation study evaluating their performance. Ecography 36, 27–46. https://doi.org/10.1111/j.1600-0587.2012.07348.x.

Ducey, M.J., 2012. Evergreenness and wood density predict height-diameter scaling in trees of the northeastern United States. For. Ecol. Manag. 279, 21–26. https://doi.org/10.1016/j.foreco.2012.04.034.

Fu, L., Duan, G., Ye, Q.L., Meng, X., Luo, P., Sharma, R.P., Sun, H., Wang, G.X., Liu, Q.W., 2020. Prediction of individual tree diameter using a nonlinear mixed-effects modeling approach and airborne LiDAR data. Rem. Sens. 12 (7), 1066. https://doi.org/10.3390/rs12071066.

Gao, X., Li, Z., Yu, H., Jiang, Z.H., Wang, C., Zhang, Y., Qi, L.H., Shi, L., 2016. Modeling of the height–diameter relationship using an allometric equation model: a case study of stands of *Phyllostachys edulis*. J. For. Res. 27, 339–347. https://doi.org/10.1007/s11676-015-0145-6.

Gao, S., Zhang, Z., 2021. Individual tree structural parameter extraction and volume table creation based on near-field LiDAR data: a case study in a subtropical planted forest. Sensors 21 (23), 8162. https://doi.org/10.3390/s21238162.

Hawbaker, T.J., Gobakken, T., Lesak, A., Tromborg, E., Contrucci, K., Radeloff, V., 2010. Light detection and ranging-based measures of mixed hardwood forest structure todd forest structure. For. Sci. 56, 313–326. https://doi.org/10.1093/forestscience/56.3.313.

Hollaus, M., Wagner, W., Maier, B., Schadauer, K., 2007. Airborne laser scanning of forest stem volume in a mountainous environment. Sensors 7, 1559–1577.

Huang, S., Titus, S.J., 1992. Comparison of nonlinear height-diameter functions for major Alberta tree species. Can. J. For. Res. 22, 1297–1304. https://doi.org/10.1139/x92-172.

Jucker, T., Caspersen, J., Chave, J., Antin, C., Barbier, N., Bongers, F., Dalponte, M., van Ewijk, K.Y., Forrester, D.I., Haeni, M., 2017. Allometric equations for integrating remote sensing imagery into forest monitoring programmes. Global Change Biol. 23, 177–190. https://doi.org/10.1111/gcb.13388.

Kankare, V., Vauhkonen, J., Tanhuanpaa, T., Holopainen, M., Vastaranta, M., Joensuu, M., Krooks, A., Hyyppa, J., Hyyppa, H., Alho, P., 2014. Accuracy in estimation of timber assortments and stem distribution - a comparison of airborne and terrestrial laser scanning techniques. ISPRS J. Photogrammetry Remote Sens. 97, 89–97. https://doi.org/10.1016/j.isprsjprs.2014.08.008.

Kearsley, E., Moonen, P.C.J., Hufkens, K., Doetterl, S., Lisingo, J., Bosela, F.B., Boeckx, P., Beeckman, H., Verbeeck, H., 2017. Model performance of tree height-diameter relationships in the central Congo Basin. Annals For. Sci. 74, 7. https://doi.org/10.1007/s13595-016-0611-0.

Latifi, H., Fassnacht, F.E., Hartig, F., Berger, C., Hernandez, J., Corvalan, P., Koch, B., 2015. Stratified aboveground forest biomass estimation by remote sensing data. Int. J. Appl. Earth Obs. Geoinf. 38, 229–241. https://doi.org/10.1016/j.jag.2015.01.016.

Lefsky, M.A., Cohen, W.B., Acker, S.A., Parker, G.G., 1999. Lidar remote sensing of the canopy structure and biophysical properties of Douglas-Fir western hemlock forests. Remote Sens. Environ. 361, 339–361.

Liang, X., 2013. Feasibility of Terrestrial Laser Scanning for Plotwise Forest Inventories. Finnish Geodetic Institute, Masala, Finland.

Liang, X., Wang, Y., Pyörälä, J., Lehtomaki, M., Yu, X.W., Kaartinen, H., Kukko, A., Honkavaara, E., Issaoui, A.E.I., Nevalainen, O., 2019. Forest in situ observations using unmanned aerial vehicle as an alternative of terrestrial measurements. For. Ecosyst. 6, 20. https://doi.org/10.1186/s40663-019-0173-3.

Liu, G., Wang, J., Dong, P., Chen, Y., Liu, Z., 2018. Estimating individual tree height and diameter at breast height (DBH) from terrestrial laser scanning (TLS) data at plot level. Forests 9 (7), 398. https://doi.org/10.3390/f9070398.

Maltamo, M., Mehtätalo, L., Valbuena, R., Vauhkonen, J., Packalen, P., 2017. Airborne laser scanning for tree diameter distribution modelling: a comparison of different modelling alternatives in a tropical single-species plantation. Forestry 91, 121–131. https://doi.org/10.1093/forestry/cpx041.

Mcroberts, R.E., Næsset, E., Gobakken, T., 2013. Remote sensing of environment inference for Lidar-assisted estimation of forest growing stock volume. Remote Sens. Environ. 128, 268–275. https://doi.org/10.1016/j.rse.2012.10.007.

Mensah, S., Pienaar, O.L., Kunneke, A., du Toit, B., Seydack, A., Uhl, E., Pretzsch, H., Seifert, T., 2018. Height-diameter allometry in South Africa's indigenous high forests: assessing generic models performance and function forms. For. Ecol. Manag. 410, 1–11. https://doi.org/10.1016/j.foreco.2017.12.030.

Meyer, H.A., 1940. A mathematical expression for height curves. J. Forecast. 38, 415–420. https://doi.org/10.1093/jof/38.5.415.

Mokroš, M., Liang, X., Surový, P., Valent, P., Cernava, J., Chudy, F., Tunak, D., Salon, S., Merganic, J., 2018. Evaluation of close-range photogrammetry image collection methods for estimating tree diameters. ISPRS Int. J. Geo-Inf. 7 (3), 93. https://doi.org/10.3390/ijgi7030093.

Moran, C.J., Rowell, E.M., Seielstad, C.A., 2018. A data-driven framework to identify and compare forest structure classes using LiDAR. Remote Sens. Environ. 211, 154–166. https://doi.org/10.1016/j.rse.2018.04.005.

Moreira, B.M., Goyanes, G., Pina, P., Vassilev, O., Heleno, S., 2021. Assessment of the influence of survey design and processing choices on the accuracy of tree diameter at breast height (DBH) measurements using UAV-based photogrammetry. Drones 5 (2), 43. https://doi.org/10.3390/drones5020043.

Muhamad-Afizzul, M., Siti-Yasmin, Y., Hamdan, O., Tan, S.A., 2019. Estimating stand-level structural and biophysical variables of lowland dipterocarp forest using airborne LiDAR data. J. Trop. For. Sci. 31, 312–323. https://doi.org/10.26525/jtfs2019.31.3.312.

Næsset, E., Gobakken, T., Holmgren, J., Hyyppa, H., Hyyppa, J., Maltamo, M., Nilsson, M., Olsson, H., Persson, A., Soderman, U., 2004. Laser scanning of forest resources: the nordic experience. Scand. J. For. Res. 19, 482–499. https://doi.org/10.1080/02827580410019553.

Ng'andwe, P., Chungu, D., Yambayamba, A.M., Chilambwe, A., 2019. Modeling the height-diameter relationship of planted *Pinus kesiya* in Zambia. For. Ecol. Manag. 447, 1–11. https://doi.org/10.1016/j.foreco.2019.05.051.

Ozkan, U.Y., Demirel, T., Ozdemir, I., Saglam, S., Mert, A., 2022. Predicting forest stand attributes using the integration of airborne laser scanning and Worldview-3 data in a mixed forest in Turkey. Adv. Space Res. 69, 1146–1158. https://doi.org/10.1016/j.asr.2021.10.049.

Parker, G.G., Harmon, M.E., Lefsky, M.A., Chen, J.Q., Van Pelt, R., Weis, S.B., Thomas, S.C., Winner, W.E., Shaw, D.C., Frankling, J.F., 2004. Three-dimensional structure of an old-growth *Pseudotsuga-Tsuga* canopy and its implications for radiation balance, microclimate, and gas exchange. Ecosystems 7, 440–453. https://doi.org/10.1007/s10021-004-0136-5.

Peereman, J., Hogan, J.A., 2022. Disturbance frequency, intensity and forest structure modulate induced changes in mangrove forest canopy cover. Global Ecol. Biogeogr. 31, 37–50. https://doi.org/10.1111/geb.13407.

Pukkala, T., Saramäki, J., Mubita, O., 1990. Management planning system for tree plantations. Silva Fenn. 24, 171–180. https://doi.org/10.14214/sf.a15573.

Puliti, S., Breidenbach, J., Astrup, R., 2020. Estimation of forest growing stock volume with UAV laser scanning data: Can it be done without field data? Remote Sens. 12 (8), 1245. https://doi.org/10.3390/RS12081245.

RIEGL, 2012. LMS-Q680i, Datasheet. RIEGL Laser Measurement Systems GmbH., Horn, Austria. http://www.riegl.com/uploads/tx_pxpriegldownloads/10_DataSheet_LMS-Q680i_28-09-2012_01.pdf. (Accessed 2 November 2022).

Saarinen, N., Kankare, V., Vastaranta, M., Luoma, V., Pyorala, J., Tanhuanpaa, T., Liang, X.L., Kaartinen, H., Kukko, A., Jaakkola, A., Yu, X.W., Holopainen, M., Hyyppa, J., 2017. Feasibility of Terrestrial laser scanning for collecting stem volume information from single trees. ISPRS J. Photogrammetry Remote Sens. 123, 140–158. https://doi.org/10.1016/j.isprsjprs.2016.11.012.

Şahin, A., Kahriman, A., Göktürk, A., 2019. Estimating diameter at breast height (DBH) from diameter at stump height (DST) in triple mixed stands in the region of Artvin in Turkey. Forestist 69, 61–67. https://doi.org/10.26650/forestist.2019.18003.

Sharma, R.P., 2009. Modelling height-diameter relationship for Chir pine trees. Banko Janakari 19, 3–9. https://doi.org/10.3126/banko.v19i2.2978.

Sharma, R.P., Vacek, Z., Vacek, S., Kučera, M., 2019. Modelling individual tree height-diameter relationships for multi-layered and multi-species forests in central Europe. Trees Struct. Funct. 33, 103–119. https://doi.org/10.1007/s00468-018-1762-4.

Silva, C.A., Klauberg, C., Hudak, A.T., Vierling, L.A., Liesenberg, V., Carvalho, S.P.C.E., Rodriguez, L.C.E., 2016. A principal component approach for predicting the stem volume in Eucalyptus plantations in Brazil using airborne LiDAR data. Forestry 89, 422–433. https://doi.org/10.1093/forestry/cpw016.

Stitt, J.M., Hudak, A.T., Silva, C.A., Vierling, L.A., Vierling, K.T., 2022. Evaluating the use of Lidar to discern snag characteristics important for wildlife. Rem. Sens. 14 (3), 720. https://doi.org/10.3390/rs14030720.

Temesgen, H., Zhang, C.H., Zhao, X.H., 2014. Modelling tree height-diameter relationships in multi-species and multi-layered forests: a large observational study from Northeast China. For. Ecol. Manag. 316, 78–89. https://doi.org/10.1016/j.foreco.2013.07.035.

Teobaldelli, M., Cona, F., Saulino, L., Migliozzi, A., D'Urso, G., Langella, G., Manna, P., Saracino, A., 2017. Detection of diversity and stand parameters in Mediterranean forests using leaf-off discrete return LiDAR data. Remote Sens. Environ. 192, 126–138. https://doi.org/10.1016/j.rse.2017.02.008.

Tompalski, P., Coops, N.C., Marshall, P.L., White, J.C., Wulder, M.A., Bailey, T., 2018. Combining multi-date airborne laser scanning and digital aerial photogrammetric data for forest growth and yield modelling. Rem. Sens. 10 (2), 347. https://doi.org/10.3390/rs10020347.

Tonolli, S., Dalponte, M., Neteler, M., Rodeghiero, M., Vescovo, L., Gianelle, D., 2011. Fusion of airborne LiDAR and satellite multispectral data for the estimation of timber volume in the Southern Alps. Remote Sens. Environ. 115, 2486–2498. https://doi.org/10.1016/j.rse.2011.05.009.

Tuan, N.T., Dinh, T.T., Long, S.H., 2019. Height-diameter relationship for *Pinus koraiensis* in Mengjiagang Forest Farm of Northeast China using nonlinear regressions and artificial neural network models. J. For. Sci. 65, 134–143. https://doi.org/10.17221/5/2019-JFS.

van Ewijk, K., Treitz, P.M., Scott, N.A., 2011. Characterizing forest succession in central ontario using Lidar-derived Indices. Photogramm. Eng. Rem. Sens. 77, 261–270. https://doi.org/10.14358/PERS.77.3.261.

Véga, C., Renaud, J., Durrieu, S., Bouvier, M., 2016. On the interest of penetration depth, canopy area and volume metrics to improve Lidar-based models of forest parameters. Remote Sens. Environ. 175, 32–42. https://doi.org/10.1016/j.rse.2015.12.039.

von Bertalanffy, L., 1949. Problems of organic growth. Nature 163, 156–158. https://doi.org/10.1038/163156a0.

White, J.C., Tompalski, P., Vastaranta, M., Wulder, M.A., Saarinen, S., Stepper, C., Coops, N.C., 2017. A model development and application guide for generating an enhanced forest inventory using airborne laser scanning data and an area-based approach. British Columbia, Victoria.

White, J.C., Wulder, M.A., Varhola, A., Vastaranta, M., Coops, N.C., Cook, B.D., Pitt, D.M., Woods, M., 2013. A best practices guide for generating forest inventory attributes from airborne laser scanning data using an area-based approach. British Columbia, Victoria.

Wu, X., Zhou, S., Xu, A., Chen, B., 2019. Passive measurement method of tree diameter at breast height using a smartphone. Comput. Electron. Agric. 163, 104875. https://doi.org/10.1016/j.compag.2019.104875.

Wykoff, W.R., Crookston, N.L., Stage, A.R., 1982. User's Guide to the Stand Prognosis Model. Gen. Tech. Rep. INT-133. U.S. Department of Agriculture, Forest Service, Intermountain Forest and Range Experiment Station, Ogden, UT.

Yang, Z., Liu, Q., Luo, P., Ye, Q.L., Duan, G.S., Sharma, R.P., Zhang, H.R., Wang, G.X., Fu, L.Y., 2020. Prediction of individual tree diameter and height to crown base using nonlinear simultaneous regression and airborne LiDAR data. Rem. Sens. 12 (14), 2238. https://doi.org/10.3390/rs12142238.

Zhang, X., Chhin, S., Fu, L., Lu, L.L., Duan, A.G., Zhang, J.G., 2018. Climate-sensitive tree height-diameter allometry for Chinese fir in southern China. Forestry 92, 167–176. https://doi.org/10.1093/forestry/cpy043.

Zhang, Z., Cao, L., Mulverhill, C., Liu, H., Pang, Y., Li, Z.Y., 2019. Prediction of diameter distributions with multimodal models using LiDAR data in subtropical planted forests. Forests 10 (2), 125. https://doi.org/10.3390/f10020125.

Zhang, Z., Cao, L., She, G., 2017. Estimating forest structural parameters using canopy metrics derived from airborne LiDAR data in subtropical forests. Rem. Sens. 9, 940. https://doi.org/10.3390/rs9090940.

Zhao, Q., Yu, S., Zhao, F., Tian, L.H., Zhao, Z., 2019. Comparison of machine learning algorithms for forest parameter estimations and application for forest quality assessments. For. Ecol. Manag. 434, 224–234. https://doi.org/10.1016/j.foreco.2018.12.019.

Zhao, X., Guo, Q., Su, Y., Xue, B., 2016. Improved progressive TIN densification filtering algorithm for airborne LiDAR data in forested areas. ISPRS J. Photogrammetry Remote Sens. 117, 79–91. https://doi.org/10.1016/j.isprsjprs.2016.03.016.

Zhao, Y., Ma, Y., Quackenbush, L.J., 2022. Estimation of individual tree biomass in natural secondary forests based on ALS data and WorldView-3 imagery. Remote Sens. 14 (2), 271. https://doi.org/10.3390/rs14020271.

Zheng, J., Zang, H., Yin, S., Sun, N.X., Zhu, P.H., Han, Y.J., Kang, H.Z., Liu, C.J., 2018. Modeling height-diameter relationship for artificial monoculture *Metasequoia glyptostroboides* in sub-tropic coastal megacity Shanghai, China. Urban For. Urban Green. 34, 226–232. https://doi.org/10.1016/j.ufug.2018.06.006.